Light sheet fluorescence microscopic imaging for the primary breakup of diesel and gasoline sprays with real-world fuels

Durst, Alexander; Wensing, Michael; Berrocal, Edouard

Published in:
Applied Optics

DOI:
10.1364/AO.57.002704

2018

Document Version:
Publisher's PDF, also known as Version of record

applied optics

Light sheet fluorescence microscopic imaging for the primary breakup of diesel and gasoline sprays with real-world fuels

Alexander Durst,[1,2,*] Michael Wensing,[1,2] and Edouard Berrocal[2,3]

[1]Institute of Engineering Thermodynamics (LTT), University of Erlangen-Nuremberg, Am Weichselgarten 8, 91058 Erlangen, Germany
[2]Erlangen Graduate School in Advanced Optical Technologies (SAOT), University of Erlangen-Nuremberg, Paul Gordan Strasse 691052 Erlangen, Germany
[3]Department of Combustion Physics, Lund Institute of Technology, Professorsgatan 1, 22100 Lund, Sweden
*Corresponding author: alexander.durst@fau.de

Received 25 January 2018; revised 1 March 2018; accepted 5 March 2018; posted 6 March 2018 (Doc. ID 320720); published 30 March 2018

This paper describes the adaptation of the laser-induced fluorescence measurement technique for the investigation of the primary breakup of modern diesel and gasoline direct injection sprays. To investigate the primary breakup, a microscopic technique is required, and with the help of special tracer dyes, a high fluorescence signal can be achieved in the visible range of the electromagnetic spectrum, resulting in good image quality with a nonintensified camera. Besides the optimization of the optical setup for the microscopic field of view, different tracer dyes are compared, and their solubility and fluorescence are tested in the desired surrogate and real-world fuels. As a tracer, the phenoxazine dye Nile Red was found to provide sufficient solubility in alkanes as well as suitable emission and excitation spectrum for the use of the second-harmonic frequency of a Nd:YAG laser (532 nm). The good quantum efficiency delivered by Nile Red also meant that single-shot images clearly showing spray structures in regions measuring up to 3 mm by 3 mm around the nozzle outlet could be recorded. Compared to relatively easy shadowgraph techniques and complex and costly x-ray synchrotron measurements, light sheet fluorescence microscopic imaging is not overly complex yet delivers excellent data on spray structures as well as qualitative fuel distribution.

OCIS codes: (300.2530) Fluorescence, laser-induced; (160.2540) Fluorescent and luminescent materials; (110.0180) Microscopy.

https://doi.org/10.1364/AO.57.002704

1. INTRODUCTION

In engine and spray research, the primary breakup of diesel and gasoline direct-injected sprays, nowadays with injection pressures of up to 250 MPa [1] for diesel and 35 MPa [2] for gasoline, is not yet fully understood. In research into primary atomization, mainly two techniques have brought about significant progress in recent years: microscopic shadowgraphy and synchrotron x-ray imaging. The typical setup for shadowgraphy measurements is usually rather simple, consisting of a light source, e.g., a flash lamp [3] or a spectral diffused laser [4], and a camera with appropriate optics.

Crua *et al.* [4] investigated the primary breakup of a modern diesel injector in the near-nozzle region during the initial state of injection using a microscopic shadowgraphy approach. The investigations showed that in the initial stage, the jet flips from laminar at 40 MPa to turbulent at 100 MPa. Moreover, their images show that at 100 MPa, the jet has very high optical density at the nozzle exit due to at least partial atomization; as a result, almost the entire jet appears black in the shadowgraph images. Only at the very edge of the spray are some structures and fluctuations in density discernible.

Reddemann *et al.* [5] developed and applied a transmitted light microscope to investigate the primary breakup of a butanol spray. They were able to show spray structures such as droplets and ligaments during the opening and closing phase of the injector and at the spray edges. Their images combine a very high resolution with very sharp depiction of the structures. However, the center of the spray remains gray and without contrast during the stationary phase of the injection due to total extinction of the transmitted light. This leads to the assumption that an investigation of the steady state of a spray is possible using shadowgraphy methods, although these are very limited in terms of the structural information that can be extracted from such images, especially in the center of the spray. Serras-Pereira *et al.* [3] used shadowgraphy to investigate the primary breakup and flash boiling in a real-size transparent gasoline injector nozzle. The use of a transparent nozzle here limits certain parameters: the maximum injection pressure is 3 MPa,

and only steady-state flows are investigated, while the transient opening and closing processes are excluded. Their results show the amount of cavitation in the nozzle as well as the resulting sprays for flash-boiling and non-flash-boiling conditions. In the gasoline spray, too, the optical density at the nozzle outlet is too high to gain insight into the spray structures in close proximity to the nozzle.

One way to overcome these difficulties of conventional shadowgraphy techniques is to use x-rays generated by a synchrotron. With x-ray techniques, three of the most relevant spray characteristics in the near-nozzle region can be investigated. X-ray absorption measurements are capable of measuring mass distributions in the near-nozzle region. Leick *et al.* [6] used this technique and showed the intense dilution of a diesel spray due to air entrainment within less than 1 mm of the nozzle exit. With single or multiple exposed x-ray phase contrast techniques, spray structures and velocity fields of near-nozzle spray structures can be captured. Zhang *et al.* [7] investigated the influence of different nozzle geometries and needle lifts on the spray structure. To do so, they used single-exposure phase-contrast imaging to capture the structures. With variations in the geometry and needle lifts, they produced completely different sprays, reaching from totally intact and undisturbed laminar jets to highly broken up, turbulent sprays. Wang *et al.* [8] used multiple exposed phase-contrast images (PCIs) to calculate the velocity of a high-speed liquid spray. Here, autocorrelation was used to derive the displacement of spray structures between two exposures and then to calculate the velocity.

Beside the opportunities offered by x-ray imaging techniques for spray diagnostics, the biggest drawback of these measurement techniques is their complexity and costs. Large electron synchrotrons typically generate the x-ray pulses required for spray investigations where experimental time is very limited and expensive. This raises the question as to whether there is a less expensive and less complex way to investigate the primary breakup that might replace the costly x-ray experiments at least in some applications.

Berrocal *et al.* [9] suggested a microscopic laser-induced fluorescence (LIF) technique that works in the visible range of the electromagnetic spectrum, light sheet fluorescence microscopic (LSFM) imaging. In this paper, we describe the adaptation and application of this technique for the very dense primary breakup region of modern gasoline and diesel injectors. Here, tracer dyes are used that can be excited by green light (532 nm) and hence fluoresce in the visible range of the electromagnetic spectrum with sufficient intensity. This intense visible fluorescence is advantageous, as nonintensified cameras can be used for signal detection, which means a significant improvement in image quality compared to intensified cameras. Though the LSFM imaging technique is more complex than conventional shadowgraphy approaches, it has its advantages. As the laser forms a light sheet, it enables the investigated area of the spray to be defined. Moreover, the signal is proportional to the fuel mass concentration, and spray structures in optical dense regions become clearly visible.

In previous work, fluorescein [10] and eosin [9,11] were used as tracer dyes. With eosin [12] being salt and fluorescein being a highly polar molecule as well, they are not soluble in the alkanes or real-world fuels that are used for this study. Besides conventional diesel and gasoline, calibration fluid ISO 4113 (as a surrogate for diesel) and n-heptane (as a surrogate for gasoline) are also investigated. To find a tracer dye that is soluble in these substances, intense literature research as well as solubility and fluorescence experiments were carried out. In addition, spray investigations in the near field of the nozzle were performed with the most promising tracer dye (Nile Red) to assess the possibilities and limits of LSFM imaging.

2. EXPERIMENTAL SETUP

A. Comparison of Different Tracer Dyes

To find a suitable tracer dye, first a number of requirements that the potential tracer dye must fulfil were defined:

- excitation spectrum with maximum excitation close to 532 nm;
- emission spectrum with a sufficiently large Stokes shift;
- good quantum yield at low concentrations;
- soluble in nonpolar substances such as alkanes;
- preferably nonhazardous.

As the laser available for this study is a frequency-doubled Nd:YAG laser, a type of laser widespread in engine research, one crucial requirement is that the tracer dye can be excited at 532 nm. A sufficiently large Stokes shift is needed to be able to cut off the excitation wavelength from the signal without losing too much signal intensity. As the tracer influences the properties of the fuel investigated, the concentration used should be as low as possible yet still have good quantum yields in order to achieve a stable signal. Moreover, all of the tracer dyes fluorescing in the visible range are solid substances. A small concentration will therefore also help to prevent deposits in the high-pressure fuel system and the injector itself. Since all of the fuels and fuel surrogates investigated are nonpolar alkanes, the tracer must be soluble in nonpolar liquids. Due to its nature as a powder, tracer residues, especially in the injection chamber and the waste air system, cannot be avoided when the fuel evaporates. Therefore, a nonhazardous dye is preferable, as this rules out hazards for staff and the environment. Based on these requirements, the tracers listed in Table 1 have been chosen from the literature search, and their solubility and fluorescence in ethanol, n-heptane, and ISO 4113 calibration fluid tested. Ethanol is used, since it served as a solvent for eosin Y salt in the measurements carried out by Storch *et al.* [11], which measurements are the starting point for this study. Moreover, the first measurements for this study carried out with ethanol and eosin Y salt as a tracer delivered good results. For this reason, the fluorescence from eosin Y is used as a reference for evaluating the other tracers. Table 1 lists all of the tracers considered with their maximum absorption and emission wavelength as well as the substance class, their polarity, and their hazardousness.

Table 1 shows that all of the dyes considered absorb in the vicinity of the desired excitation wavelength of 532 nm from the frequency-doubled Nd:YAG laser. Moreover, the signals emitted from all the tracer dyes have a sufficient Stokes shift of at least 17 nm, allowing separation from the laser wavelength. With the exception of the two rhodamine derivatives,

Table 1. Peak Absorption Wavelength (PAW) and Peak Emission Wavelength (PEW), Substance Class, Polarity, and Hazardousness of the Tracer Dyes Considered

Tracer	PAW [nm]	PEW [nm]	Substance Class	Polarity	Hazard
Eosin Y	525 [13]	543 [13]	Xanthen [13]	Polar	slight [12]
Rubrene	538 [14]	555 [14]	Polycyclic aromatic hydrocarbon [15]	Nonpolar	slight [15]
Macrolex	535 [16]	584 [16]	Coumarin [16]	Slightly polar	none [17]
Nile Red	484–591 [18]	529–657 [18]	Pheno-xazin [18]	Slightly polar	none [19]
Rhodamine 6G	530 [20]	552 [20]	Xanthen [20]	Polar	High [21]
Rhodamine B	543 [22]	565 [22]	Xanthen [22]	Polar	High [23]

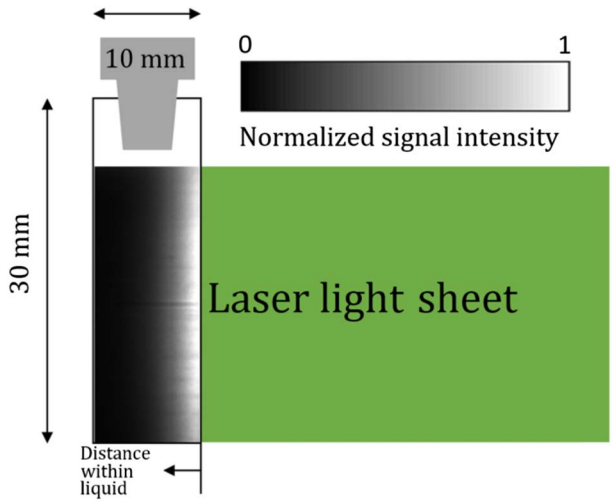

Fig. 1. Schematic of the cuvette containing the fuel tracer solution, illuminated with a green light sheet from the right. An exemplary fluorescence raw signal distribution is seen in the cuvette.

all of the dyes have an acceptable level of hazardousness. For Nile Red, it is noticeable that its absorption and emission peak vary across a wide range. This is because the higher the polarity, the more redshifting occurs in the two peaks. According to Greenspan and Fowler [18], for Nile Red with n-heptane as a solvent, the excitation maximum is 484 nm and the emission maximum 529 nm. Small amounts of ethanol (0.1%–1%) added to a heptane solution of Nile Red result in a redshift in the emission maximum of up to 50 nm.

To find the best tracer dye for the desired LSFM imaging technique, tests of solubility, as well as fluorescence experiments, are carried out. For eosin Y, besides the salt, both the free acid and a solution of salt and 20% propanol are tested. To examine the fluorescence, a cuvette is filled with the tracer-fuel solution and illuminated by a light sheet from the Nd:YAG laser. The resulting fluorescence signal is captured using a non-intensified camera. Figure 1 shows a schematic of the setup for the fluorescence tests with the cuvette containing the fuel-tracer solution illuminated by a laser light sheet coming from the right-hand side. In the cuvette, an image of a raw fluorescence signal distribution is shown, as captured by the camera and subsequently processed.

From the fluorescence images recorded, the mean value is computed column-wise and plotted over the propagation distance in the liquid. Because ethanol with 60 mg/l eosin Y salt is used as the reference, all fluorescence signals are normalized to its intensity.

B. Spray Investigations

To carry out the LIF spray measurements, gasoline and diesel research injectors are used. For gasoline, a solenoid actuated injector from the XL3.1 series from Continental was chosen. For good optical access to the single spray cone, a three-hole nozzle with a spray hole diameter of 170 µm without counter bores is used. The cones are inclined at an angle of 30° from the injector length axis and are equidistantly allocated over the circumference, which leads to an angle between them of 120°. The injector is energized for 1.5 ms for each injection.

The diesel injector is a servo-hydraulic piezo common rail injector from the PCRs2 series from Continental. This is also designed as a three-hole research injector with a spray hole diameter of 114 µm, an l/d ratio of 6.5 and a conicity factor of 2. Its holes are inclined at an angle of 45° from the injector length axis (umbrella angle of 90°) and also equidistantly allocated over the circumference. This injector is energized for 1.0 ms for each injection. For both injectors in this study, the fuel is injected at room temperature.

To supply the injectors with fuel, two purpose-built pressure pulsation-free fuel systems are used. Each of them works with two air-fuel pressure intensifiers. The gasoline fuel system is capable of supplying pressures up to 28 MPa, and the diesel system can generate a maximum pressure of 400 MPa.

The injectors are mounted in a spray chamber on the underside, and optical access is available on three sides. While the laser light sheets are coupled into the spray through both side windows, the spray images are captured through the front window. Figure 2 shows a cross section of the computer-aided design (CAD) model of the injection chamber.

The figure shows the gasoline injector, mounted on the underside. To avoid signal loss due to absorption, the light sheet is coupled in through both side windows, cutting through the spray cone. The cone investigated is the one pointing to the right. A Quanta-Ray PIV400 laser system is used to generate the light sheet. This Nd:YAG laser is designed mainly to generate two consecutive laser pulses for particle image velocimetry from two independent cavities. For this LIF application, the pulse delay is set to 0, meaning a single pulse with a duration of approximately 8 ns and a pulse energy of 700 mJ is generated. The laser has an initial beam diameter of 9 mm and a beam divergence <0.5 mrad. Together with the width and height of the light sheet of 0.2 mm by 15 mm, this leads to an average laser power density of approximately 1900 kW/cm^2 within the light sheet. The second-harmonic

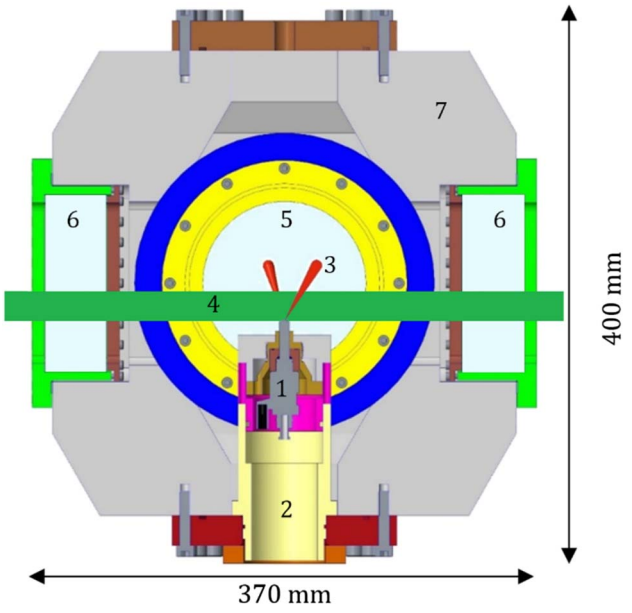

Fig. 2. Section through the CAD model of the used spray chamber with the gasoline injector mounted from below. Components: injector (1), injector mounting (2), spray cone (3), laser light sheet (4), front window (5), side windows (6) and chamber body (7).

frequency of the laser is used for these measurements, resulting in an output wavelength of 532 nm.

To form two light sheets and couple them into the chamber from both sides, the optical setup shown in Fig. 3 is utilized.

The Nd:YAG laser emits the beam, and a pinhole cuts the Gaussian beam profile to a near "top-hat" profile. After passing through a 50/50 beam splitter, the resulting beams are directed by the mirrors. The mirror setup provides identical lengths of the optical path for both light sheets. Different optical path lengths turned out to lead to a very uneven distribution of intensity for both beams due to absorption and divergence. Each of the last mirrors directs the respective beam through a telescope, consisting of horizontally and vertically aligned Kepler telescopes comprising cylindrical lenses, into the spray chamber. The vertical telescope provides a constant height of 15 mm for the light sheet, while the horizontal telescope forms a beam waist of approximately 200 µm (i.e., in the range of the nozzle diameter) in the measurement volume. The fluorescence signal is captured by a K2 DistaMax long-distance microscope from Infinity and a Sensicam (gasoline) or a pco.2000 (diesel), each from PCO. The long-distance microscope is set to a magnification of 5. With the 2048 pixel × 2048 pixel resolution of the pco.2000, a single image represents 3 mm × 3 mm. Each pixel thus covers an area of 1.5 µm × 1.5 µm. For the Sensicam, the microscope is set to a magnification of 3.3, meaning each image represents 2 mm × 2.5 mm. With the Sensicam's resolution of 1280 pixels × 1024 pixels, each pixel represents an area of 2 µm × 2 µm. The magnifications are chosen to capture the aforementioned areas of interest. Theoretically higher magnifications can also be achieved with this setup. To cut off the laser light from the signal, a 532 nm notch filter is mounted between the camera and the long-distance microscope (not shown in Fig. 3).

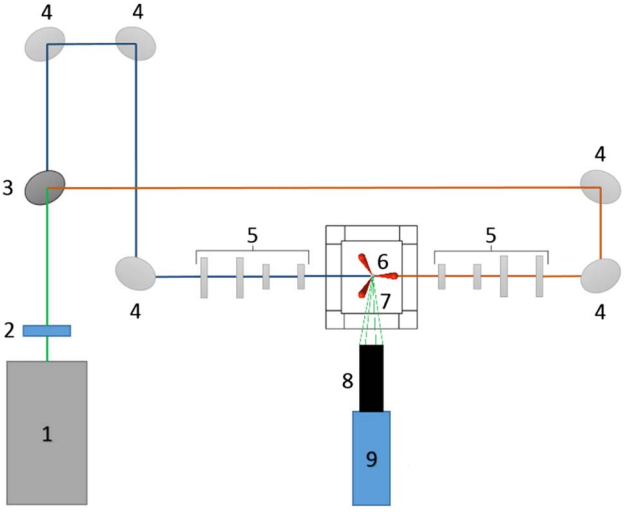

Fig. 3. Optical setup used to form and couple in the laser light sheets and capture the images. Components: laser (1), pinhole (2), 50/50 beam splitter (3), mirrors (4), telescope (5), spray chamber with investigated spray (6), fluorescence signal (7), long distance microscope (8), and camera (9).

3. RESULTS AND DISCUSSION

A. Comparison of Different Tracer Dyes

Figure 4 shows the fluorescence signals of all the tested tracers dissolved in n-heptane and ethanol with 60 mg/l eosin Y salt. Each signal is normalized to the peak fluorescence intensity of the ethanol-eosin solution. To achieve sufficient solubility of eosin Y salt and eosin Y free acid in n-heptane, 20 vol% propanol for salt and 10 vol% propanol for free acid have to be added. The concentration of tracer dye for these solutions refers to the whole mixture.

The diagram clearly shows the high fluorescence of eosin Y salt in ethanol combined with very high absorption with

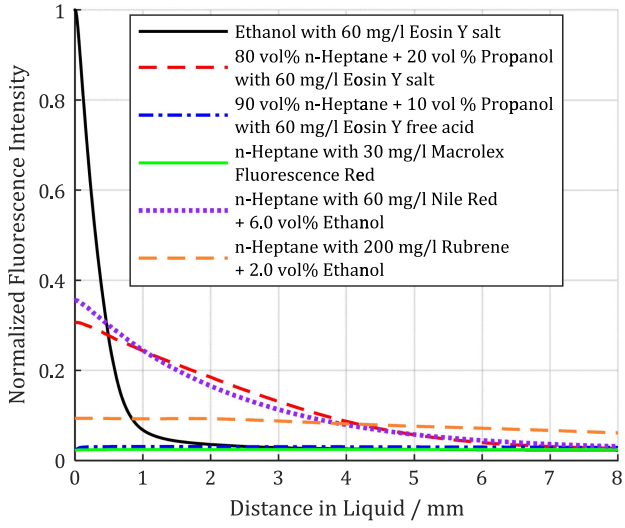

Fig. 4. Normalized fluorescence signals from all the tracer dyes in n-heptane.

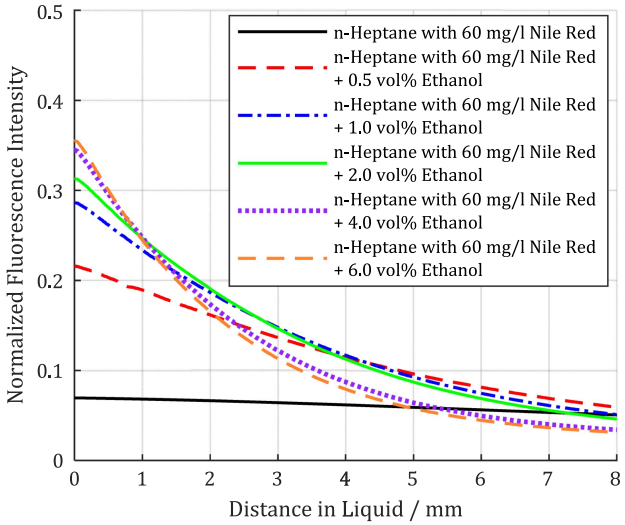

Fig. 5. Normalized fluorescence signals for n-heptane with Nile Red and ethanol contents from 0 up to 6 vol.%.

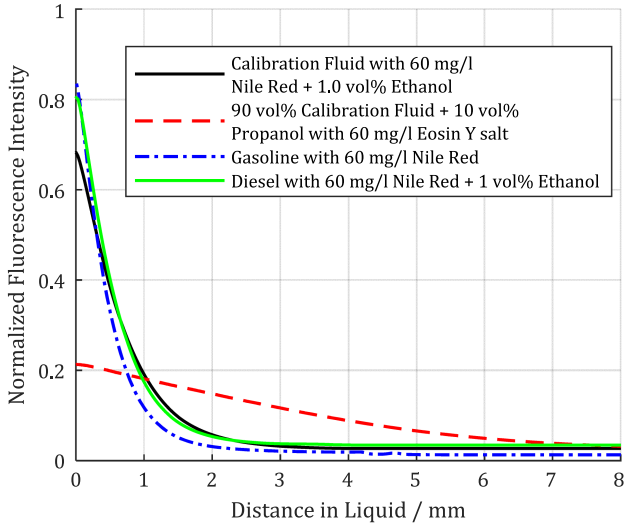

Fig. 6. Normalized fluorescence signals of calibration fluid with Nile Red, eosin Y salt and eosin Y free acid as well as gasoline and diesel with Nile Red.

increasing distance within the liquid. From the investigated tracers in n-heptane, only eosin Y salt and Nile Red show significant fluorescence. Eosin Y free acid, Macrolex Fluorescence Red and rubrene show virtually no significant fluorescence signal or absorption. As for eosin Y salt, 20 vol.% of propanol has to be added to achieve solubility; this is not further considered below, as this high amount of propanol leads to a significant change in the fuel properties of n-heptane or any other fuel or fuel surrogate. Hence, Nile Red can be determined as the most suitable tracer for n-heptane, as it is nontoxic, has a good quantum yield, and requires only 2 vol% of ethanol to be added, which means very little fuel dilution.

Greenspan and Fowler [18] found that the spectrum of Nile Red in n-heptane, on the one hand, is extremely dependent on the amount of ethanol added. On the other hand, they state that ethanol quenches the fluorescence signal. To find the optimum, an experiment was carried out to investigate this dependency in the present case. Figure 5 shows the normalized fluorescence signals of n-heptane with Nile Red containing ethanol amounts from 0 up to 6 vol%.

The diagram clearly shows that pure n-heptane with Nile Red shows no significant fluorescence when excited with light at a wavelength of 532 nm. Even as little as 0.5 vol% ethanol leads to 3 times the signal intensity. Adding more ethanol results in a steady but digressive increase in signal intensity. The best compromise between signal intensity and fuel dilution was found to be 2 vol% of ethanol. This composition is therefore used for the following spray measurements. Though the diagrams show 8 mm distance in liquid, the desired spray experiment will have spray hole diameters of under 200 µm, which means absorption in liquid will play a minor role.

Besides the tests in the pure substance n-heptane, the most promising dyes were also tested in ISO 4113 calibration fluid, which is a multicomponent petroleum distillate. Figure 6 shows the results for Nile Red and eosin Y salt. Due to the better solubility of eosin Y salt in this multicomponent substance, only 10% of propanol had to be added here to achieve sufficient solubility of the eosin dye. In addition, the results for normal diesel and gasoline with Nile Red are also illustrated.

For the multicomponent substance calibration fluid, Nile Red with 1% of ethanol was found to produce very good results, with a relative fluorescence signal of almost 70% of the reference. This is due to the slight polarity of calibration fluid leading to a redshift in the signal, which is in accordance with the reported behavior of the fluorescence signal for increasing amounts of ethanol. Moreover, it turns out that the tracer dye Nile Red is also suitable for real-world fuels like gasoline and diesel with normalized fluorescence signals of more than 80%. For gasoline, which contains up to 5 vol% of ethanol in Germany, no further ethanol has to be added. For diesel, 1 vol% of ethanol turns out to be enough for the same reasons as for calibration fluid. Eosin Y salt shows significantly higher signal intensities than in a solution with n-heptane. However, the eosin tracer dye exhibits a far lower fluorescence intensity than the mixtures containing Nile Red. Furthermore, with a content of 10 vol% of propanol, considerable dilution of the base fuel is still necessary to achieve solubility. The generally higher fluorescence intensities for the real-world fuels are caused by the higher solubility of the tracer dyes in the multicomponent substances compared to the pure n-heptane. For calibration fluid, fluorescence was also tested without a tracer. This test showed no detectable fluorescence in this setup. Table 2 summarizes the results, giving an overview of the dyes tested and their solubility, as well as their fluorescence in ethanol, n-heptane, and calibration fluid.

For a deeper comparison of the different tracer dyes solved in the different fuels, the graphs from Fig. 4–6 have been fitted according to the following equation:

$$F(x) = c \cdot f \cdot e^{-c \cdot x \cdot \epsilon}. \quad (1)$$

F is the normalized fluorescence intensity, f is a measure for the specific fluorescence, c is the concentration of the tracer

Table 2. Overview of the Tested Dyes and their Solubility as Well as their Fluorescence in Ethanol, n-Heptane, and Calibration Fluid[a]

Tracer	Solubility Ethanol	Fluorescence Ethanol	Solubility n-Heptane	Fluorescence n-Heptane	Solubility Calibration Fluid	Fluorescence Calibration Fluid
Eosin Y salt	+	+	–	x	–	x
Eosin salt + 10 vol.%/20 vo.l% propanol	x	x	o	o	o	o
Eosin Y free acid + 10 vol.% propanol	x	x	–	–	–	o
Rubrene	x	x	+	–	x	x
Macrolex	x	x	o	–	+	–
Nile Red + 1 vol.%/2 vol% ethanol	x	x	+	o	+	+

[a]x, not tested; +, good; o, intermediate; –, poor.

Table 3. Tracer Fuel Mixtures with their Absorption Coefficient ε and Relative Fluorescence Intensity f

Tracer Fuel Mixture	Relative Fluorescence f	Absorption Coefficient ε
Ethanol with eosin Y	1	2.71
80 vol.% n-heptane + 20 vol.% propanol with eosin Y	0.35	0.28
n-heptane with 0.5 vol.% ethanol	0.24	0.15
n-heptane with 1.0 vol.% ethanol	0.29	0.23
n-heptane with 2.0 vol.% ethanol	0.31	0.27
n-heptane with 4.0 vol.% ethanol	0.34	0.39
n-heptane with 6.0 vol.% ethanol	0.35	0.43
Calibration fluid with Nile Red	0.71	1.43
90 vol.% calibration fluid + 10 vol.% propanol with eosin Y	0.26	0.18
Gasoline with Nile Red	0.88	2.06
Diesel with Nile Red	0.85	1.73

dye, x the distance in liquid, and ε the absorption coefficient. As except for Macrolex and rubrene, the concentration is the same for all probes, it is set to a value of 1 to achieve direct comparability between the coefficients and the figures. For eosin-free acid, Macrolex, rubrene, and n-heptane with 0 vol%, there is no detectable fluorescence. Hence, no fit is possible, and they are not included in Table 3.

The table clearly shows that the promising tracer dyes have a high relative fluorescence intensity and that high fluorescence intensities accompany high absorption coefficients.

B. Spray Investigations

Using the experimental setup described and Nile Red as a tracer dye, spray investigations were carried out for the diesel injector with ISO 4113 calibration fluid and 60 mg/l Nile Red + 1 vol% ethanol and for the gasoline injector with n-heptane and 60 mg/l Nile Red + 2 vol% ethanol. Since the laser used has a pulse repetition frequency of 15 Hz, only one picture per spray event can be captured. Hence, all following sequences show single-shot images of different spray events. Figure 7 depicts a study of the opening process of the diesel injector. All images shown in the following section are raw images; to the LSFM images a color map has been applied.

A thin, protruding jet is visible 10 µs after the visible start of injection (VSOI). This jet consists of fuel from a previous injection that is left in the spray hole being pushed out by the current injection. The developing jet forms a mushroom-like shape 20 µs after VSOI, due to fuel shearing off the spray tip. At 30 µs after VSOI, fuel formerly located at the spray tip has thus moved to the sides of the spray. In the subsequent period, the front of the spray leaves the 3 mm × 3 mm image region, and the spray continues to develop. Spray structures are also clearly visible in these images using a non-intensified camera and the short laser pulse length; they are depicted very clearly and nonblurred. These images provide an insight into the dense spray in the nozzle near region using the LSFM imaging technique. Internal structures become visible, as does the qualitative fuel mass distribution. During injector opening, an initial accumulation of fuel with a high fuel concentration is ejected. This accumulation is followed by a jet with less fuel. When the spray becomes stationary, an area of a high fuel concentration is formed at the injector, which is diluted very quickly downstream in the spray.

Figure 8 shows the first 30 µs after VSOI in higher temporal resolution. The images shown in this case are from one single spray event, again at 100 MPa fuel pressure, 0.1 MPa ambient pressure, and with calibration fluid.

They were captured using a Kirana High-Speed Camera at 5 million fps. Here, too, a long-distance microscope was utilized. The shadowgraph images were illuminated by a flash lamp and show the same phenomena as the LIF images. Since a laser is not necessarily needed for shadowgraphy images, high-speed image sequences can be easily recorded and are only limited by the frame rate provided by the camera. Thanks to the higher frame rate and the fact that a single spray event can be investigated, an insight into the dynamic processes can be gained.

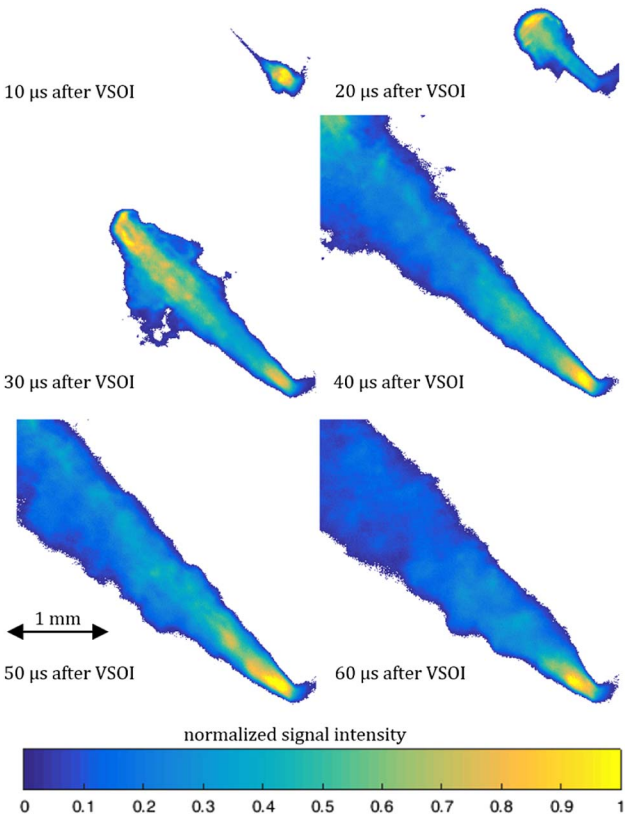

Fig. 7. LSFM study of the opening process of the diesel injector at 100 MPa injection pressure and 0.1 MPa ambient pressure with calibration fluid from 10 to 60 µs after the VSOI (selected single-shot images of different injections).

The protruding jet can also be seen in this spray event, even 30 µs after VSOI. The formation of the mushroom-like structure 20 µs after VSOI is also present here and is sheared to the sides of the spray by the subsequent fuel. In the shadowgraph images, another interesting phenomenon occurs between 12 and 18 µs after VSOI. At 12 µs, another ball-shaped fuel structure leaves the injector. Until 15 µs, it grows in size before it starts to catch up with the spray front. After 18 µs, it reaches the tip of the spray, subsequently becoming the new spray front. On the other hand, the main disadvantage of the shadowgraphy technique becomes obvious here. Due to the high optical density of the spray, only the outer boundary is depicted. The inside of the spray, including the inner structures, remain invisible.

In addition to injector opening, the steady-state phase of injection is also investigated. Figure 9 shows six images from different spray events, each taken 600 µs after the VSOI to investigate cyclic fluctuations in the injection process.

These six selected images from different spray events clearly show the highly stochastic character of the spray. The upper images show a very narrow and concentrated spray with a small cone angle, while the middle images show a wider spray, and the lower images depict a clearly less concentrated and wide spray with a large cone angle. All images show a short, intact core of approximately one spray hole diameter in length. This

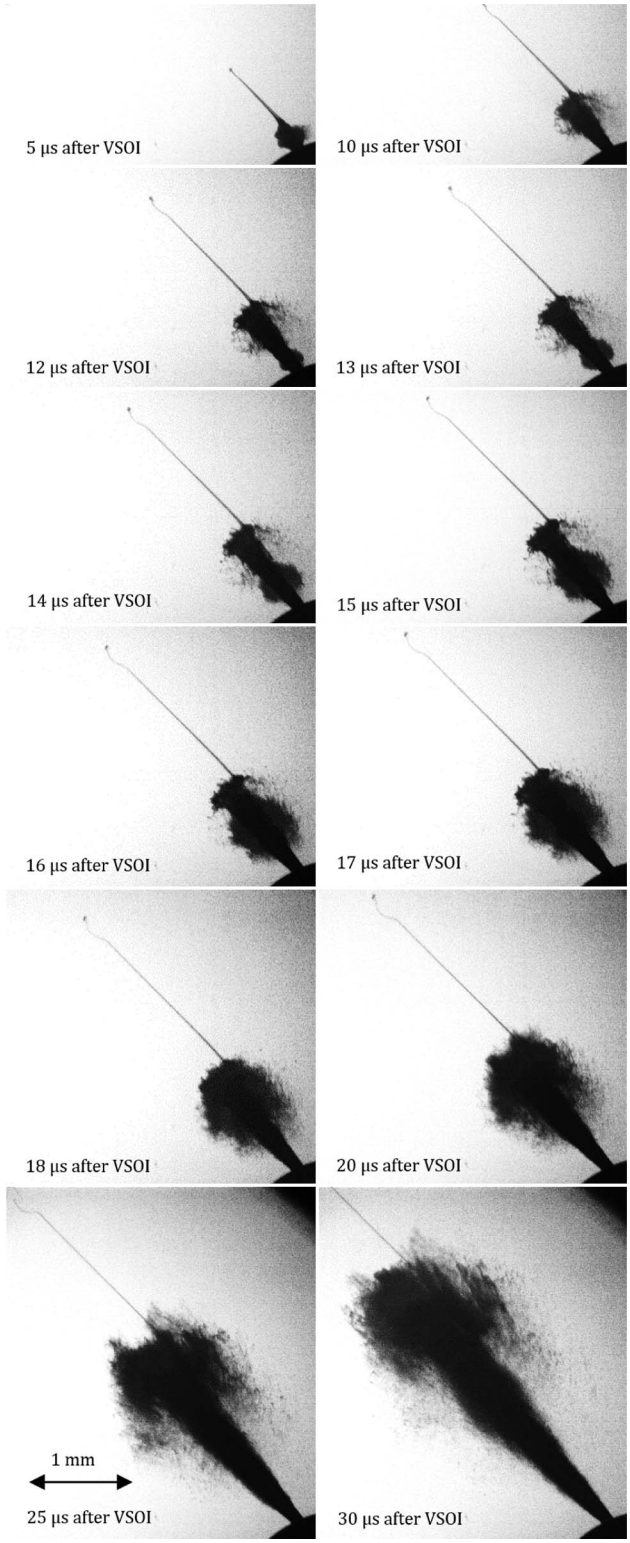

Fig. 8. Shadowgraphy study of the opening process of the diesel injector at 100 MPa fuel pressure and 0.1 MPa ambient pressure with calibration fluid from 5 to 30 µs after the VSOI at ultrahigh speed (5 million fps).

core then breaks up, diluting very quickly with the surrounding air. Figure 10 shows a single LSFM image on the left and an x-ray PCI on the right.

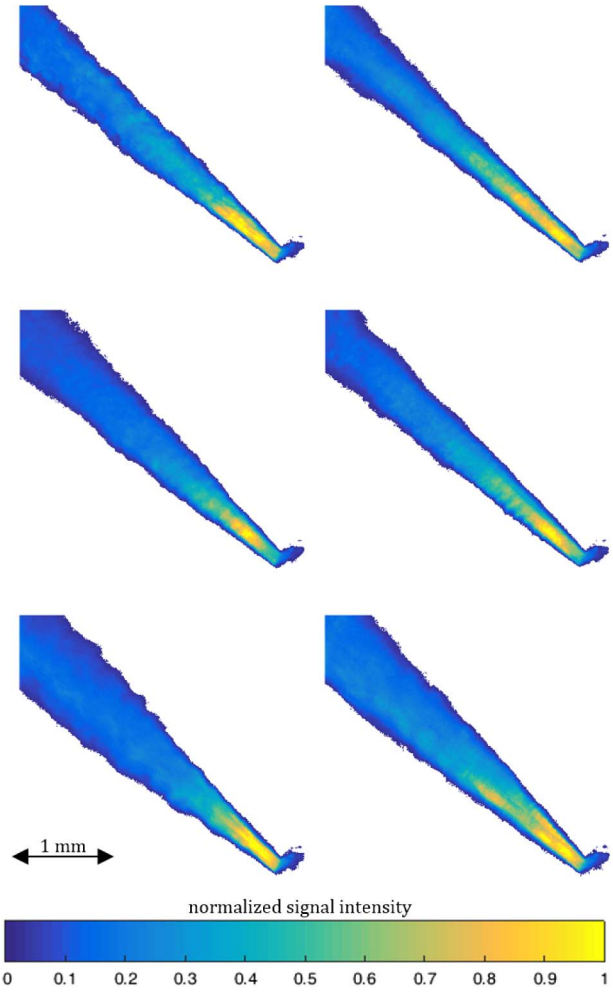

Fig. 9. LSFM single-shot images from six different spray events all taken 600 μs after VSOI with the diesel injector at 100 MPa injection pressure and 0.1 MPa ambient pressure with calibration fluid (selected single-shot images from different injections).

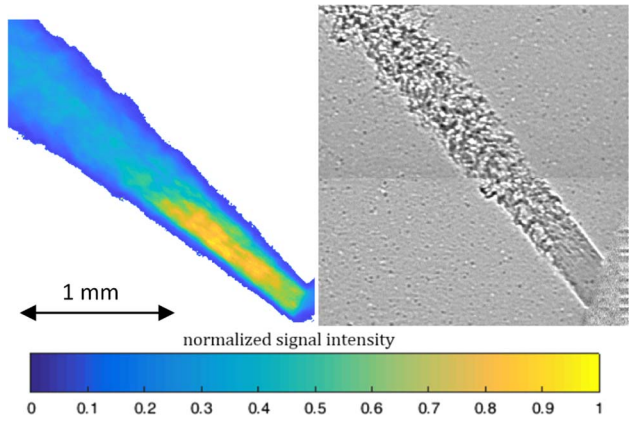

Fig. 10. LSFM single-shot image(left) and x-ray PCI (right) of the same spray, both 600 μs after VSOI with the diesel injector at 100 MPa injection pressure and 0.1 MPa ambient pressure with calibration fluid.

The direct comparison of both techniques with a higher zoom into the images clearly shows the intact liquid core in the PCI and also in the LSFM image a very even and smooth surface can be found within the first hole diameter after the nozzle. Moreover, in Fig. 10 an anomaly of the LIF signal can be observed. As soon as the jet starts to disintegrate, the signal rises before it decreases again. This anomaly is presumably due to the surface of the jet. As the surface starts to disintegrate, multiple scattering of the signal and the laser leads to higher signal intensity, though there is no increase in fuel density. This effect impedes a quantitative evaluation of the signal in terms of fuel density within the light sheet. A first evaluation, assuming the LIF signal is proportional to the fuel density in the light sheet, shows an underestimation of the density in the area of the intact jet of approximately 30% to 40%, combined with nonrealistic structures.

To verify the applicability of the LSFM imaging technique for gasoline direct injection (GDI) injection processes as well, Fig. 11 shows the opening process of the gasoline injector with n-heptane as fuel, an injection pressure of 20 MPa and an

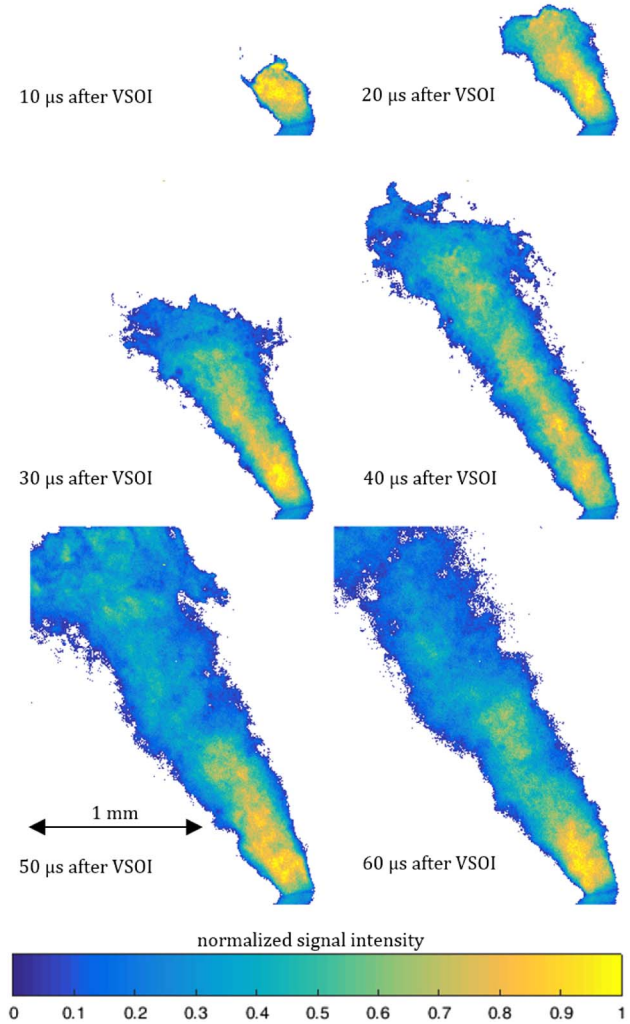

Fig. 11. LSFM study of the opening process of the GDI injector at 20 MPa injection pressure and 0.1 MPa ambient pressure with n-heptane from 10 to 60 μs after the VSOI (selected single-shot images from different injections).

ambient pressure of 0.1 MPa. Once again, the images depicted are taken from single-spray events.

The LSFM imaging technique very clearly and sharply depicts the developing spray structures from the spray center to the outer edge for the opening process of the GDI injector as well.

In Fig. 12, a direct comparison between LSFM imaging and scattered light imaging is given. Both images are captured with the same setup, only removing the notch filter and not adding tracer dye for the scattered light image. The dots of high intensity clearly show the different character of both techniques. While LFSM gives a concentration or volume proportional signal, scattered light gives a surface proportional signal, highlighting single, big droplets as areas with high signal intensity. Comparing both images, the LSFM image shows a more even distribution of intensity and allows more insight into inner spray structures. Moreover, the glare points, which are present in the scattered light image, drive out the camera easily, leading to a poor depiction of smaller droplets.

For the GDI injector, the opening process is shown in shadowgraphy images of higher temporal resolution in Fig. 13. Once again, a high-speed camera in combination with a long-distance microscope was used for image acquisition. The surrogate fuel in these experiments was iso-octane.

The shadowgraphy images show a very similar contour of the developing spray compared to the LIF technique. The spray starts as a mushroom-like shape. The head then is sheared off to the sides. This is particularly visible on the right of the spray. This shearing causes the spray to change from a mushroom-like spray to more of a cone-like shape before it leaves the region of interest. The structures at the edge of the spray appear very similar with both techniques. But even for the less dense GDI spray, it is obvious that only the LSFM imaging technique is capable of delivering a clear insight into the spray.

In Fig. 14, six single images from different spray events at 600 μs after VSOI are displayed for the GDI injector. The injection parameters are the same as for the study of the injector opening using LSFM imaging (20 MPa injection pressure and 0.1 MPa ambient pressure with n-heptane).

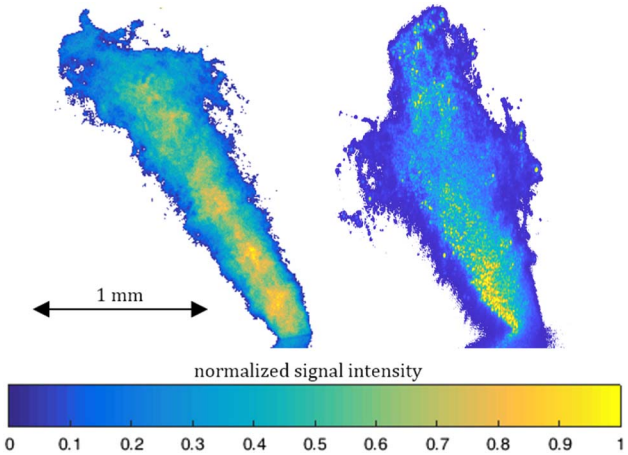

Fig. 12. Comparison of a fluorescence image (left) to a light-scattering image (right) with the same setup. Image is taken 40 μs after VSOI during the opening process of the GDI injector at 20 MPa injection pressure and 0.1 MPa ambient pressure with n-heptane.

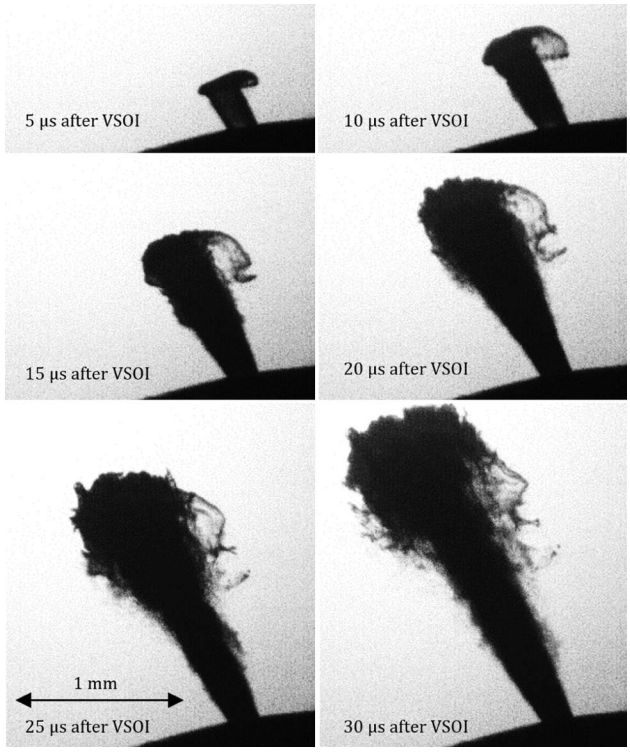

Fig. 13. Shadowgraphy study of the opening process of the GDI injector at 15 MPa fuel pressure and 0.1 MPa ambient pressure iso-octane 5–30 μs after the VSOI at ultrahigh speed (5 million fps).

For the GDI injector, once again the selected images from different cycles clearly show the stochastic character of the spray. Compared with the diesel injector, however, the shape of the spray is more reproducible, and fewer fluctuations in shape occur. Moreover, a far wider spray with a bigger cone angle exits the injector.

In the GDI case, a normalized intensity of 1 correlates with approximately 200 counts. This means 5% of the 12-bit dynamic of the Sensicam has been used. For the diesel injector, the maximum number of counts is 1000; thus, 6% of the 14-bit dynamic has been used.

Comparing the two breakup mechanisms of diesel and gasoline sprays, significant differences are apparent. Although the pressures used in diesel injection are an order of magnitude higher, the spray leaves the injector as an intact jet, which starts to disintegrate after exiting the nozzle. This breakup mechanism is also described by Shi *et al.*, who investigated the primary breakup of a diesel injector by means of x-ray phase contrast and large eddy simulation [24]. In contrast, the gasoline spray already splits up into ligaments when leaving the injector and is significantly wider then the diesel spray. This splitting at the nozzle outlet is due to massive cavitation inside the spray hole and its lower guidance by the spray hole. This was also demonstrated by Bornschlegel *et al.* by means of shadowgraphy in a real-size glass nozzle [25]. Furthermore, from the very beginning, the spray appears to be significantly wider than the diesel spray and thus dilutes faster (note the different scale of the images). Though the overall fluorescence intensity of the GDI spray is lower due to the lower intensity of

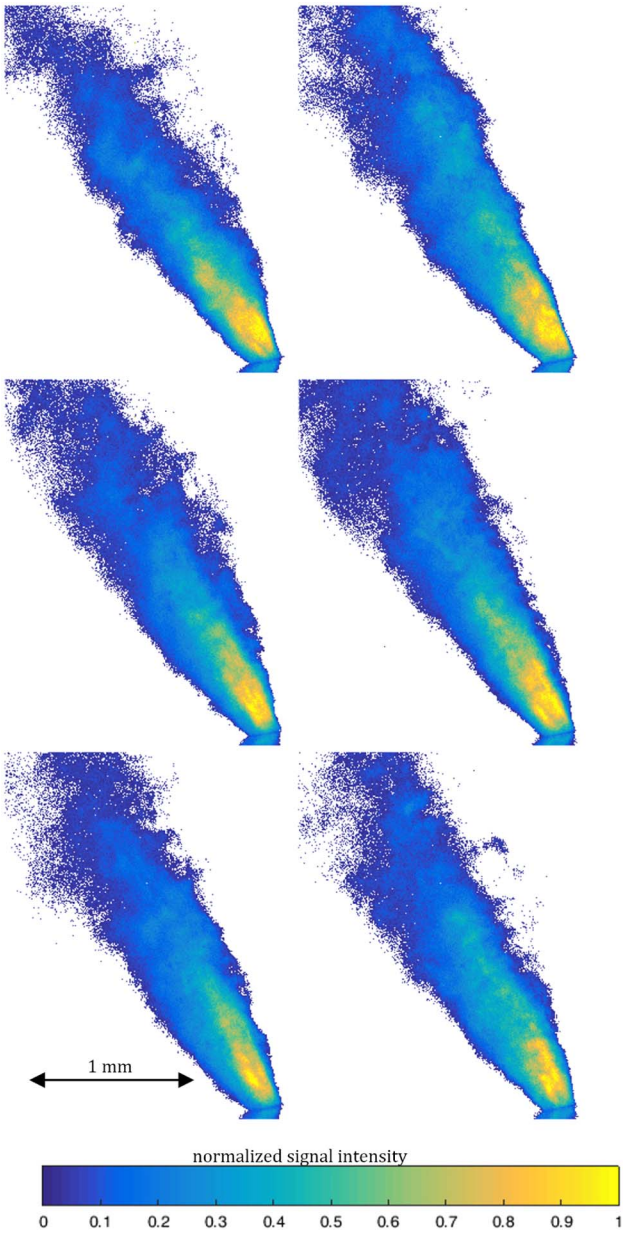

Fig. 14. LSFM single images from six different spray events all taken 600 µs after VSOI with the GDI injector at 20 MPa fuel pressure and 0.1 MPa ambient pressure with n-heptane (selected single-shot images from different injections).

the n-heptane solution, nonetheless, it is remarkable that the GDI spray is barely detectable anymore at 2 mm from the nozzle; the diesel spray still is very dense and narrow.

4. CONCLUSIONS

By testing and comparing several tracer dyes, the phenoxazine dye Nile Red is identified as well soluble in nonpolar, alkane surrogate, and real-world fuels. With fluorescence tests, it shows a good quantum yield and a well-suited spectrum for the desired LSFM imaging technique with a frequency-doubled Nd:YAG laser and a nonintensified camera. Experimental spray investigations confirmed the suitability of Nile Red for observing the primary breakup of modern diesel as well as GDI injectors. The spray measurements show a sufficiently high signal intensity, which allows for the use of a nonintensified camera even with a long-distance microscope with a magnification of up to 5. By using the nonintensified camera, the resulting spray images show the structure of the spray as well as its qualitative mass distribution very clearly and in detailed form. A comparison with ultra-high-speed shadowgraphy image sequences reveals the same spray phenomena and demonstrates the high image quality and insight into the spray gained using the LSFM imaging technique. Moreover, the LSFM imaging technique is capable of showing the different breakup mechanisms for both injector types. Fuel leaves the diesel injector as a liquid jet, which starts to disintegrate outside the injector. The GDI injector produces a spray that has already disintegrated and fissured as it leaves the nozzle due to cavitation inside the nozzle.

5. OUTLOOK

From those results, where a tracer for alkane fuels is found and the capability of the LSFM imaging technique depicting primary structures is demonstrated, the next steps have to be taken. First, for future investigations, engine-relevant conditions have to be reached. This means for the diesel injector in particular, reaching higher gas density, i.e., higher ambient pressure and also higher ambient temperature. For the GDI injector, the investigation of flash boiling conditions is especially relevant, i.e., subatmospheric pressure and hot fuel lead to superheated fuel in reference to the ambient conditions.

Another important step to be taken is a further investigation of the described signal anomaly enabling improved validity in the quantitative evaluation of the fuel density in the light sheet. Therefore, a detailed characterization of the emission and absorption spectra is planned as well as a deeper understanding of the phenomena leading to the signal anomaly has to be gained by further isolated experiments.

Moreover, investigating the in-nozzle flow in real-sized glass nozzles will help link primary spray structures with phenomena occurring inside the nozzle.

Finally, the presented approach can be combined with structured laser illumination planar imaging (SLIPI) for suppressing the intensity contribution from multiple light scattering and to obtain quantitative results [26]. However, it should be noted that the refraction of light inside irregular liquid bodies such as ligaments and large liquid structures would limit the SLIPI technique in the near-nozzle region. A promising alternative approach to reduce multiple light scattering and compensate for light attenuation effects is to generate and detect two-photon fluorescence using femtosecond laser pulses. The authors are currently investigating this approach.

Funding. IGF project 18958 N/2, Forschungskuratorium Maschinenbau e.V.–FKM; Erlangen Graduate School of Advanced Optical Technologies (SAOT); Deutsche Forschungsgemeinschaft (DFG); H2020 European Research Council (ERC) (638546-ERC).

Acknowledgment. The authors gratefully acknowledge financial support for parts of their work from the Erlangen Graduate School in Advanced Optical Technologies (SAOT) within the framework of the German Excellence Initiative by the German Research Foundation (DFG). E. Berrocal's research activity is funded by the European Research Council (ERC) under the European Union's Horizon 2020 Research and Innovation Programme. Moreover, the authors would like to thank Specialized Imaging Limited for providing the Kirana UHS camera and support for the measurements. Special thanks go to Markus Schwarzhuber and Stevan Jestrovic for their help developing the setup and running the experiments in the context of their theses.

REFERENCES

1. Robert Bosch GmbH, "Druck beim Diesel: Warum eine Drucksteigerung Sprit spart und gleichzeitig Leistung und Drehmoment erhöht," http://www.bosch-presse.de/pressportal/de/de/druck-beim-diesel-42396.html.
2. T. Pauer, H. Yilmaz, J. Zumbrägel, and E. Schünemann, "New generation Bosch gasoline direct-injection systems," MTZ Worldwide **78**, 16–23 (2017).
3. J. Serras-Pereira, Z. van Romunde, P. G. Aleiferis, D. Richardson, S. Wallace, and R. F. Cracknell, "Cavitation, primary break-up and flash boiling of gasoline, iso-octane and n-pentane with a real-size optical direct-injection nozzle," Fuel **89**, 2592–2607 (2010).
4. C. Crua, T. Shoba, M. Heikal, M. Gold, and C. Higham, "High-speed microscopic imaging of the initial stage of diesel spray formation and primary breakup," in *SAE 2010 Powertrains Fuels & Lubricants Meeting*, SAE Technical Paper Series, Warrendale, Pennsylvania (2010).
5. M. A. Reddemann, F. Mathieu, and R. Kneer, "Transmitted light microscopy for visualizing the turbulent primary breakup of a microscale liquid jet," Exp. Fluids **54**, 1607 (2013).
6. P. Leick, A. L. Kastengren, Z. Liu, J. Wang, and C. F. Powell, "X-ray measurements of mass distributions in the near-nozzle region of sprays from standard multi-hole common-rail diesel injection systems," in *11th Triennial International Annual Conference on Liquid Atomization and Spray Systems (ICLASS)* (2009).
7. X. Zhang, S. Moon, J. Gao, E. M. Dufresne, K. Fezzaa, and J. Wang, "Experimental study on the effect of nozzle hole-to-hole angle on the near-field spray of diesel injector using fast X-ray phase-contrast imaging," Fuel **185**, 142–150 (2016).
8. Y. Wang, X. Liu, K.-S. Im, W.-K. Lee, J. Wang, K. Fezzaa, D. L. S. Hung, and J. R. Winkelman, "Ultrafast X-ray study of dense-liquid-jet flow dynamics using structure-tracking velocimetry," Nat. Phys. **4**, 305–309 (2008).
9. E. Berrocal, E. Kristensson, and L. Zigan, "Light sheet fluorescence microscopic imaging for high-resolution visualization of spray dynamics," Int. J. Spray Combust. Dyn. **10**, 86–98 (2017).
10. Y. N. Mishra, F. Abou Nada, S. Polster, E. Kristensson, and E. Berrocal, "Thermometry in aqueous solutions and sprays using two-color LIF and structured illumination," Opt. Express **24**, 4949–4963 (2016).
11. M. Storch, Y. N. Mishra, M. Koegl, E. Kristensson, S. Will, L. Zigan, and E. Berrocal, "Two-phase SLIPI for instantaneous LIF and Mie imaging of transient fuel sprays," Opt. Lett. **41**, 5422–5425 (2016).
12. Pubchem Open Chemistry Database, "Acid Red 87," https://pubchem.ncbi.nlm.nih.gov/compound/11048#section=Top.
13. Fluorophores, "Eosin Y," http://fluorophores.tugraz.at/substance/460.
14. L. Ma, K. Zhang, C. Kloc, H. Sun, M. E. Michel-Beyerle, and G. G. Gurzadyan, "Singlet fission in rubrene single crystal: direct observation by femtosecond pump-probe spectroscopy," Phys. Chem. Chem. Phys. **14**, 8307–8312 (2012).
15. Pubchem Open Chemistry Database, "5,6,11,12-tetraphenylnaphthacene," https://pubchem.ncbi.nlm.nih.gov/compound/68203#section=Top.
16. Fluorophores, "Macrolex Fluorescence Red G," http://www.fluorophores.tugraz.at/substance/598.
17. Lanxess, "Sicherheitsdatenblatt MACROLEX Fluoreszenzrot G," http://www.shanghaiguanan.com/pic/20148517229943.pdf.
18. P. Greenspan and S. D. Fowler, "Spectrofluorometric studies of the lipid probe, nile red," J. Lipid Res. **26**, 781–789 (1985).
19. Pubchem Open Chemistry Database, "Nile Red," https://pubchem.ncbi.nlm.nih.gov/compound/65182#section=Top.
20. Fluorophores, "Rhodamine 6G," http://www.fluorophores.tugraz.at/substance/504.
21. Acros Organics BVBA, "Material safety data sheet rhodamine 6G: rhodamine 6G," http://www.clayton.edu/portals/690/chemistry/inventory/MSDS%20Rhodamine%206G.pdf.
22. Fluorophores, "Rhodamine B," http://www.fluorophores.tugraz.at/substance/505.
23. Carl Roth GmbH + Co KG, "Sicherheitsdatenblatt: Rhodamin B (C.I. 45170) für die Mikroskopie," https://www.carlroth.com/downloads/sdb/de/T/SDB_T130_DE_DE.pdf.
24. J. Shi, P. Aguado Lopez, E. Gomez Santos, N. Guerrassi, G. Dober, W. Bauer, M.-C. Lai, and J. Wang, "Evidence of vortex driven primary breakup in high pressure fuel injection," in *28th European Conference on Liquid Atomization and Spray Systems (ILASS)* (2017).
25. S. Bornschlegel, C. Conrad, and A. Durst, "Multi-hole gasoline injection: in-nozzle flow and primary breakup investigated in transparent nozzles and with x-ray," in *Motorische Verbrennung. Aktuelle Probleme und moderne Lösungsansätze: (XIII. Tagung): Tagung im Haus der Technik, Ludwigsburg, 16./17. März 2017 = Engine Combustion Processes* (ESYTEC Energie- und Systemtechnik GmbH, 2017), pp. 361–372.
26. E. Berrocal, E. Kristensson, P. Hottenbach, M. Aldén, and G. Grünefeld, "Quantitative imaging of a non-combusting diesel spray using structured laser illumination planar imaging," Appl. Phys. B **109**, 683–694 (2012).